Marine Research
of the National Academy of Marine Research
ISSN: 2709-6629 (Vol.2 Iss.1)
GPN: 2011200033

DOI: http://dx.doi.org/10.29677/MR.202206_2(1).0002
2022, 2(1), 9-22

Development of Recognition Technology for the Shoreline Extraction of Waisanding Sandbar in Satellite Images

Hsien-Kuo Chang [1] Wei-Wei Chen [1*] Jin-Cheng Liou [1]
Yung-Fang Chiu [2] Wen-Chang Yang [3] Meng-Syue Li [3]

[1] *Department of Civil Engineering, National Yang Ming Chiao Tung University, Taiwan*
[2] *National Academy of Marine Research, Taiwan*
[3] *Division of Marine Science and Information Research Center, National Academy of Marine Research, Taiwan*

ABSTRACT

The Waisanding sandbar has suffered from continuous beach erosion and is gradually disappearing. It is necessary and urgent to solve this problem under the homeland protection policy. We have provided a satellite-image-based solution for this problem. We found that the northern end of the Waisanding sandbar has been reduced by 2.1km in the past 15 years, and the southern end has been significantly shortened and rotated counterclockwise. Since 2011, the southern tip has been submerged in the water, and gradually disappeared at the average tide level. Three kinds of convolutional neural network were established to identify the sea and land near the Waisanding sandbar. VGG16UNET with an identification accuracy of higher than 90% was examined to be superior to the other two Waisanding sandbar models. VGG16UNET can effectively distinguish the sea and land areas covered by thin clouds and is applicable to the land areas that are not in the training group.

Keywords: image recognition, convolutional neural network, shoreline change.

* Corresponding author, E-mail: steve.cv90g@nctu.edu.tw

Received 3 November 2021, Accepted 8 March 2022.

1 INTRODUCTION

From the past in Taiwan, there have been many research documents analyzing the shoreline changes of the Waisanding sandbar (hereinafter abbreviated as WSD), such as Wu et al. (1991), Chang and Chen (2005), Su et al. (2006), Lin et al. (2007), Tsai et al. (2015), Chang et al. (2017), Peng et al. (2019). All the results showed the long-term shrinkage and land migration of WSD. But the different image resolutions and research periods of these results are main reasons for the difference in the movement speed of the shoreline on the sea side of WSD With the government's efforts to restore the natural coastal environment, reduce disasters and coastal land loss, and implement the goal of sustainable coastal development, this research hopes to introduce high-precision satellite images and efficient artificial intelligence (AI) technology to improve the existing analysis method and to analyze the changes of WSD.

The development of satellite image-processing technology enables researchers to quickly obtain a wide range of surface information on the earth and apply it to research in different fields, such as Kurosawa and Tanaka (2001), Ryu et al. (2008) and Gilvear et al. (2004). Some results by Gardel and Gratiot (2005), Ryu et al. (2002), specially investigated shoreline changes based on satellite images. To be able to compare and analyze satellite images at different times, one needs to consider the tide level at the time the image was taken and the slope of the sea bottom. The waterline acquired in a satellite image should be corrected to the same reference at the average tide level for subsequent analysis. Based on the corrected waterline in different satellite images Boak and Turner (2005), Gardel and Gratiot (2005), Chen and Chang (2009) investigated shoreline changes at some chosen sites. The methods of acquiring waterlines in images can be divided into three categories: 1. Threshold value method; 2. Image classification method, and 3. Boundary detection method. The more representative studies using the threshold method are Jishuang and Chao (2002). Dewi et al. (2016), who used the threshold value method of pixel-value classification. Ghoneim et al. (2015) and Bayram et al. (2015) considered the image classification of spectral distribution of different light bands and spatial textures. Chen and Chang (2009) and Toure et al. (2018) used the boundary detection method to study shoreline changes. In addition to the above classification, there are also cases where various methods are combined. Fuse and Ohkura (2018) developed a waterline extraction method for SAR images, using machine learning of spatial patterns to decompose the image into its textural and contour components. Then, the non-local mean filter is used to smooth the contour image. Finally, image cutting technology is used to segment the image into ocean and land areas.

Different from the unsupervised model of the traditional image processing method, the supervised model, if it can be established through the labeling data of manual judgment, can reduce the error caused by the different hues. Foody (2006) used multi-layer perceptron (MLP) to identify target patterns in the satellite different images. Zhang et al. (2013) used satellite image data to determine the beach line location through PCA principal component analysis and SVM (support vector machine) classification algorithm. In traditional machine learning methods, such as MLP and SVM, each observed data is for each pixel, and the model established is only a more complex or non-linear threshold judgment for hue in which surrounding features are not considered. The part of land or sea in controversial surrounding features, such as whitecaps and intertidal zones, are manually marked.

Among the commonly used neural network structures, the Convolutional Neural Network (CNN) is most recently used to deal with image recognition problems. This network structure can achieve recognition capacity by marked features. If the network structure is deepened, the feature loss caused during the connection of each layer can be reduced. Traditional convolutional neural networks have been developed and applied to different fields, such as VGG of Simonyan and Zisserman (2014), Resnet (Deep residual network) of He et al. (2016), FCN (Fully Convolutional Networks) of Long et al. (2015), and U-net of Ronneberger et al. (2015). Subsequent research on image object segmentation are also based on Unet for further extensions such as Shvets et al. (2018)

Marine Research of the National Academy of Marine Research
DOI: 10.29677/MR.202206_2(1).0002

and Cheng et al. (2016). Li et al. (2018) compared the recognition capacity of SeNet, SegNet, and DeepUNet of the same image. Dickens et al. (2019) modified the original DeepUNet of Li et al. (2018) by increasing the DownBlock layers.

Based on the previous work on recognition techniques by CNN, this study aims to compare the recognition capacity of UNet, DeepUNet, and VGG16UNet for the shoreline extraction of Waisanding Sand Bar in satellite images.

2 MATERIALS ANS METHODS

2.1 Study Site

The study site, WSD, is the largest sandbar in Taiwan. It extends from the coast of Hukou Village in Yunlin to the southwest to the sea off of Wangliao Village in Chiayi. It is 12.6 kilometers long, and its land area is about 12.5 square kilometers at low tide (about -1.2m relative to the average water level). Figure 1 shows the location in a cut and reproduced Google Earth map from 2020.

Figure 1. Location of Waisanding sandbar in a cut and reproduced Google Earth map from 2020.

The Central Meteorological Bureau (CWB) analyzed the mean high and low water levels of all tide stations. There are four tide stations outside WSD. From the website of CWB the average tidal range of Boziliao, Dongshi, Budai stations in the north and of Jiangjun station in the south is 220cm, 152cm, 149cm, 135cm and 113cm, respectively. The average tidal range of these stations shows a decreasing trend from north to south. During the period from the southwest monsoon to the northeast monsoon, the observed offshore wave heights of WSD are relatively large. The main wave heights are between 50-150 cm on average, and the main period is between 4-7 sec. The main wave heights in Budai Port waters average 35-63 cm, and the main periods are between 4-9 sec. In the sea area near Budai Port, the wave heights gradually increase from north to south. The main wave heights are about 25-40 cm in the Haomili section and about 50-175 cm in the Shuangchun section in the south.

Marine Research of the National Academy of Marine Research
DOI: 10.29677/MR.202206_2(1).0002

2.2 Image data and processing

We collected 25 satellite images in different seasons over the past 15 years while also considering the clear recognizability of the waterline in the image, and the other time when the image was taken for the tide at mean water level. In the former consideration the lower cloud cover and wide distribution affect the waterline extraction less. The main consideration of the latter is to reduce the method error caused by the correction of the tide position from the waterline to the shoreline. Chang and Chen (2005) indicated that the position of extracted waterline varies with tides and waves. The tidal level at the time when a selected image was taken is close to the mean water level. Then extracted waterline slightly deviates from the shoreline. The geometric correction by sea bottom slope should be performed to shift the waterline to the shoreline at the mean water level.

After the appropriate image is selected, image processing to obtain the waterline in an image involves four steps, which are (1) radiometric correction and relative radiometric correction; (2) calculate the normalized difference water index (NDWI) to convert image information; (3) image enhancement and repair, including satellite image IHS fusion and image enhancement; and (4) morphology combination operations such as expansion or erosion.

2.3 Convolutional neural network

We referred to the model structure of U-Net in the previous studies to establish an applicable U-Net network to extract the waterline in a satellite image. When constructing the model, Leaky ReLu is used in the activation function in the U-Net internal network to avoid the disappearance of the gradient, and the sigmoid function is used as the activation function in the final estimation layer in response to the classification of sea and land. Following the common settings of parameters, we set the learning rate to 0.0001, epochs to 40, and batch size to 5.

Convolutional Networks for Biomedical Image Segmentation is the earliest U-net model proposed by Ronneberger et al. (2015). Figure 2 shows the U-net structure, the shape of which is similar to the English letter U. It was originally used for cell cutting, and was later widely used in various types of image segmentation.

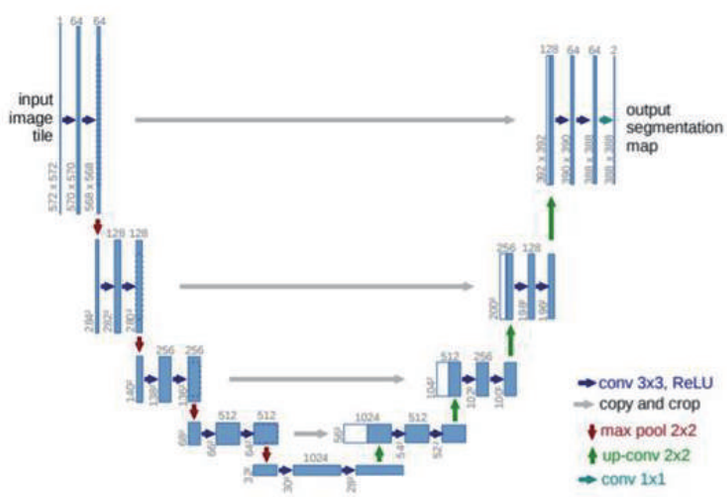

Figure 2. Structure diagram for U-Net. (Ronneberger et al., 2015)

Marine Research of the National Academy of Marine Research
DOI: 10.29677/MR.202206_2(1).0002

Li et al. (2018) proposed a deepening of the original Unet model, called DeepUNet, to separate the land and sea areas in both satellite images and aerial images. The model structure is shown in Figure 3.

VGG16 (Visual Geometry Group Network) was proposed by Simonyan and Zisserman (2014). Each block structure of VGG16 is composed of three series of convolutions plus maxpooling, which can avoid over-fitting and reduce the amount of parameters in a deeper network. Because it is a deeper convolutional neural network (CNN), the corresponding view field in the output layer is wide, which means that each pixel of each prediction corresponds to wider range in origin input.

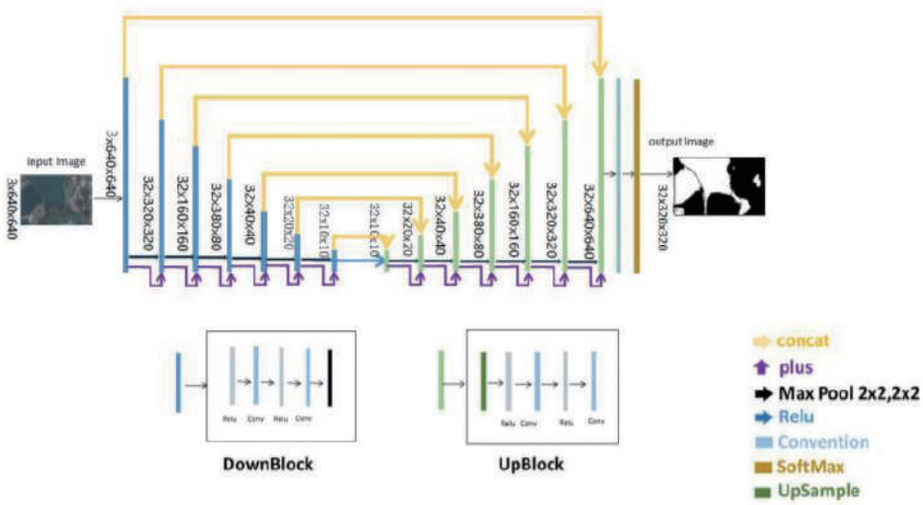

Figure 3. Structure diagram for DeepUNet. (Li et al., 2018)

2.4 Index of model evaluation

In the deep learning model, most of the neural network models are commonly used. In the neural network model, the network model is successively trained through the update of the weight values obtained by minimizing the error between predictions and targets. The function for calculating this error is called the loss function, so the decision of the loss function is very important for model training.

Both Dice loss and Focal loss were used in this study. Dice loss is the loss function proposed by Milletari et al. (2016) in V-net. Dice loss is equal to 1-F score. F score is defined as Eq. (1) and simultaneously corresponds to the accuracy rate and recall rate. The values of P (precision) and R (recall) are defined in Eq. (2), where *TP*, *FP*, *TN* and *FN* are shown in the confusion matrix of Table 1, also known as an error matrix. If the inference result of each calculation unit in Table 1 is judged to be positive or negative, it shows that the calculation result of this unit corresponds to the ground truth as True or False, respectively. From the accumulated TP, FP, TN and FN within a certain range, the P and R within the range can be calculated, and the F-score can then be obtained. The higher the F value, the more accurate the recognition ability of the model.

DOI: 10.29677/MR.202206_2(1).0002

The IOU Score (Intersection Over Union) is also often used as a reference for accurate evaluation of image segmentation. The definition of the IOU is the ratio of the area of overlap to the area of union for both the ground-truth set and prediction set. The higher the IOU value, the more accurate the recognition ability of the model.

$$\frac{1}{F}=\frac{1}{P}+\frac{1}{R}\rightarrow \quad F=\frac{PR}{P+R} \tag{1}$$

$$P=\frac{TP}{TP+FP},\quad R=\frac{TP}{TP+FN} \tag{2}$$

Table 1. Confusion matrix in loss function.

Ground-truth	**Prediction**	
	Positive	Negative
Truth	*TP*	*FN*
False	*FP*	*TN*

3 RESULTS AND DISCUSSION

3.1 Ground-truth images and shoreline changes

The 25 collected images are SPOT 5 and SPOT 6 satellite images. The pre-processing method described in the previous section is used to acquire the shoreline in each selected appropriate image. Three wavebands, green light, red light, and near-infrared light (NIR) in image information are used to determine the shoreline of each image. The 25 obtained ground-truth images for WSD only, excluding the land area of the island of Taiwan, are shown in Figure 4. Gray scale for WSD in Figure 4 is white, and the other part is black. Due to the different pixel resolutions of various satellite images, the images are resized to a resolution of 2.5m through cubic polynomial interpolation in order to unify the spatial scale of the identification model.

The shoreline of each image with the same resolution of 2.5 m from 2005 to 2020 is drawn as shown in Figure 5. The blue line for 2005 is gradually changed to red for 2020, showing the shoreline changes of WSD over the past 15 years. It can be seen from Figure 4 that the length of WSD has been shortened year by year. The northern end has been reduced by 2.1km over the past 15 years, and the southern end has been significantly shortened and rotated counterclockwise. Since 2011, the southern tip has been submerged in the water and gradually disappeared at the average tide level.

Marine Research of the National Academy of Marine Research
DOI: 10.29677/MR.202206_2(1).0002

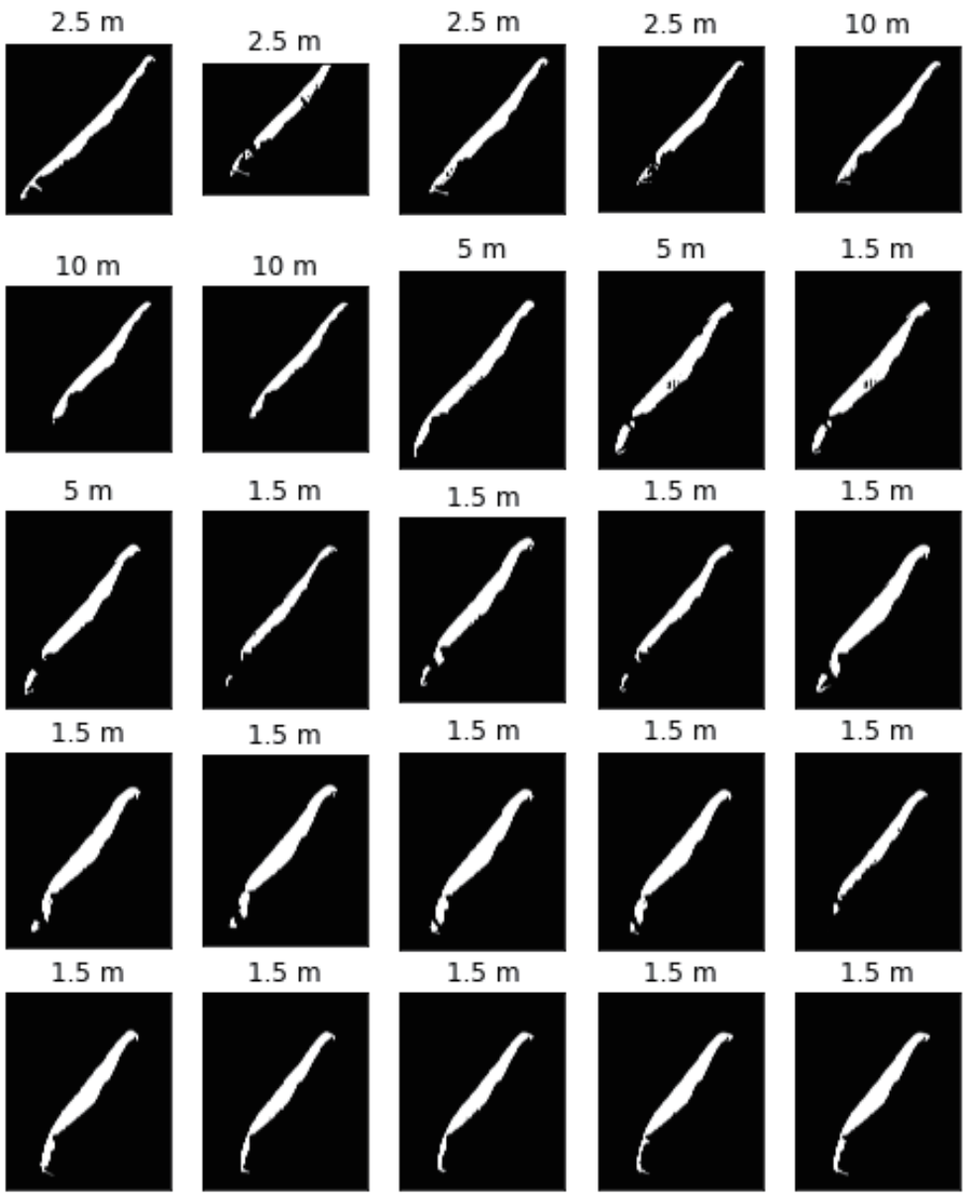

Figure 4. Twenty-five ground-truth images from 2005 to 2020.

Marine Research of the National Academy of Marine Research
DOI: 10.29677/MR.202206_2(1).0002

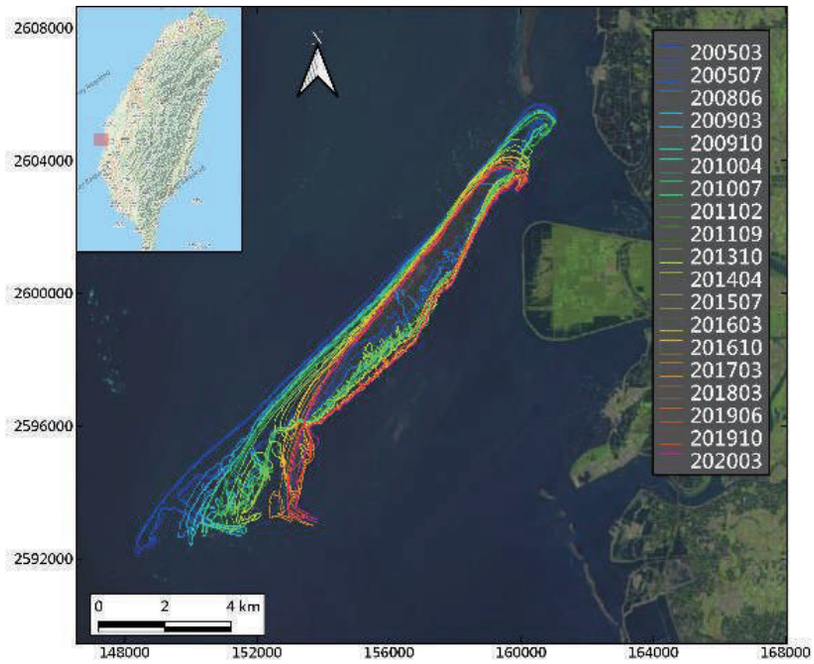

Figure 5. The shoreline changes of WSD from 2005 to 2020.

3.2 Training of AI recognition model

In addition, to increase the training data set, the picture is rotated every 20 degrees a total of 18 times before sampling, which can increase the amount of data by 18 times. The construction of deep learning models generally uses an image processor (GPU) to accelerate the training process. The neural network needs to fix the size of the input image. The input data size of the network model constructed in this study is 256*256*3, that is, the image is cut into units of 256*256. After cutting, we check whether the input image and labeling data are correct, as shown in Figure 6.

After cutting the sample image in Figure 6, it can be found that most of the data in the image is sea area data. To avoid the influence of too much sea area data on waterline recognition, and since the purpose of this research is to judge the sea area and the land area, the whole sea area and the whole land area are excluded before inputting the training model. There are 24,551 cut images remaining. All data is divided into training data set, validation data set, and test data set according to the common ratio of 70%, 20%, and 10%, respectively. The numbers of training data set, validation data set, and test data set are 17,185, 4,910, and 2,456, respectively.

In the field of image recognition, deep learning includes object detection and segmentation. When training models, image enhancement techniques are often used to compensate for insufficient data and can effectively avoid overfitting. It includes rotation, offset, zoom, affine conversion, horizontal and vertical flip, adding noise, etc. Through these techniques, each training data set can be variegated to increase the training data set and avoid the effect of over-learning.

However, the data argumentation techniques induce several meaningless values in bordering zone. When training VGG16UNet for this type of identification study, the Loss obtained increased from 0.07 to 0.38, and the IOU Score decreased from 0.91 to 0.64. The result shows that that the image enhancement technology is not suitable for identification of WSD.

DOI: 10.29677/MR.202206_2(1).0002

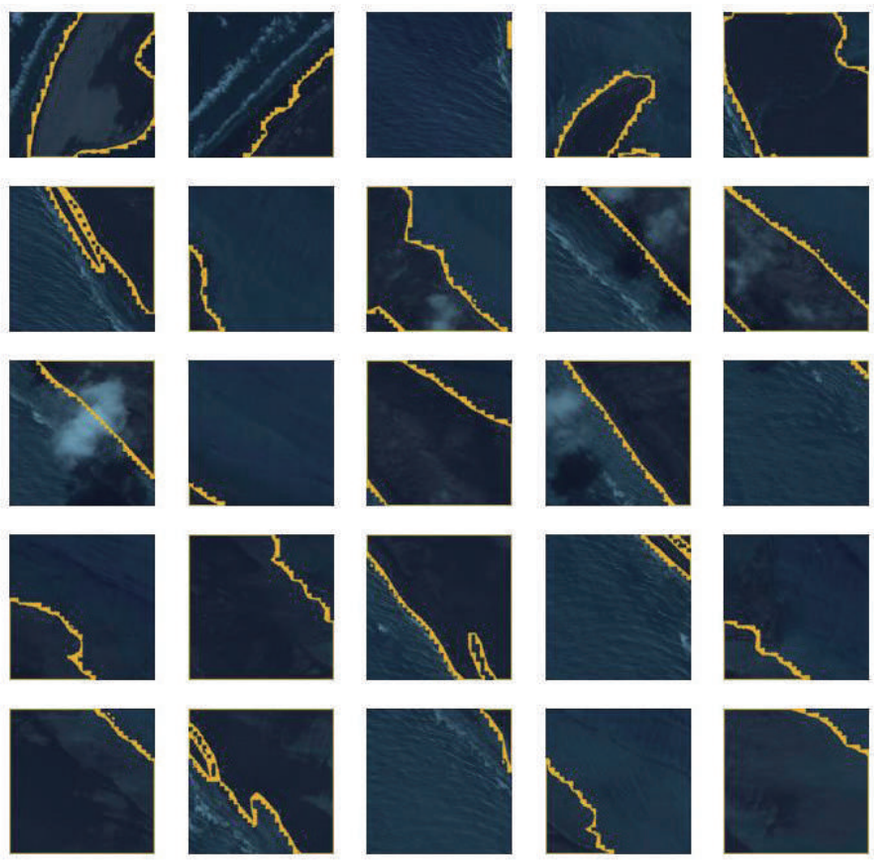

Figure 6. The comparison between labeling result and original image.

The model evaluation results of the test data after the model training has been completed are shown in Table 2. The loss index in Table 2 includes dice-loss and focal loss together. Table 2 shows that VGG16 has the best performance among three examined models, with a loss of 0.07, an IOU score of 0.91, and an F score of 0.95.

The three network models have high recognition capabilities to distinguish most of the land and sea locations, but some of them still contain noise. Deeper networks often have whole slice recognition errors inside WSD, resulting in hollow pictures.

Table 2. Indexes of model evaluation in test data set.

model	Loss	IOU score	F score
U-Net	0.125	0.876	0.920
DeepUNet	0.117	0.879	0.922
VGG16UNet	0.070	0.917	0.950

3.3 Effect of cloud cover

Several ground-truth images with clouds are difficult to identify manually. Each model is applied to the identification and comparison of images with higher clouds, as shown in Figure 7, which indicates that

DOI: 10.29677/MR.202206_2(1).0002

VGG16UNet has a better performance in the identification of cloudy conditions than the other two models. There are many incorrect recognition areas in various models, for example in image no. 7, as shown in Figure 8. To explore its possible causes, we compared the band analysis of three better samples and one poor sample in the identification of cloudy conditions. Figure 9 indicates that the spectrum of the green light band of image no. 7 is obviously more concentrated, and the average brightness of the three bands is also higher than that of the other three images.

Figure 7. Comparison of the results of three modes to identify images under cloudy conditions (left to right: original image, U-Net, DeepUNet, VGG16UNet).

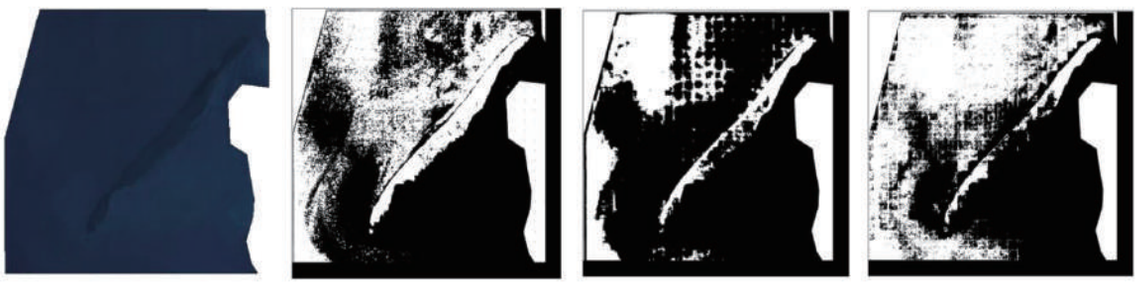

Figure 8. An example of serious misidentification for three modes (left to right: original image, U-Net, DeepUNet, VGG16UNet).

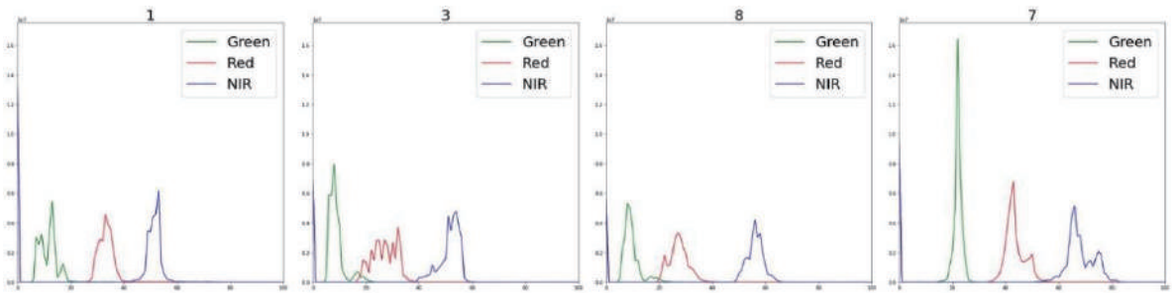

Figure 9. Band analysis of four samples in cloudy conditions (left to right: image number 1, 3, 8, 7).

Marine Research of the National Academy of Marine Research
DOI: 10.29677/MR.202206_2(1).0002

From comparison of the above results, it can be known that VGG16UNet has a high recognition ability and can be adapted to even cloudy images. However, sometimes, results that have misjudgment in the identification of the whole land area may be caused by the removal of the data samples of the whole sea area and the whole land area simultaneously during training. It is recommended that the sample selection of various images should be appropriately evaluated when training the model in the future. In addition, VGG16UNet can identify the land type data that has not been trained, as shown in Figure 10. The white area on the right side of Figure 10 is the agricultural land of Aogu Village in Taiwan. Although this area is excluded in the model training stage, it still is identified as land by VGG16UNet. This result shows that VGG16UNet has superior sea and land recognition capabilities. If other more complex land data is added to the training, and more types of land learning materials are used, the model should be able to effectively understand the characteristics of the sea area and increase identification ability. As for the problem that most models misjudge sample number 7, it is recommended that more images with different illumination and atmospheric conditions can be added as training data to improve the recognition accuracy.

Figure 10. Original image of sample number 1 (left) and identified result by VGG16UNet (right).

The equipment required to build this AI model is a CPU using Intel i7-9700F, RAM64G, and GPU using RTX 2080s. UNet and DeepUNet training time is about 3 hours, VGG16UNet training takes longer, about 4 hours. At present, VGG16UNet will have poor results for specific sunlight or images with special spectral performance. Generally, the green light, red light and infrared light spectrum provided by satellite images can be saved as PNG image files to quickly capture the land and sea location.

At present, VGG16UNET only has poor recognition of specific sunlight or images with special spectra. If PNG formatted satellite image files were inputted that generally contain green, red and infrared light, VGG16UNET can quickly recognize the position of land and sea. The results can provide other subsequent advanced engineering and scientific applications.

4 CONCLUSIONS

WSD has suffered from continuous beach erosion and gradually disappearing for decades. Because traditional topographic surveying requires time and effort, long-term and regular observational data are not available for understanding the mechanism of its beach change. Extracting the waterline in multiple available satellite images is another way to solve this problem. 25 collected SPOT 5 and SPOT 6 satellite images in

DOI: 10.29677/MR.202206_2(1).0002

different seasons from 2005 to 2020 are resized to have ground-truth images with the same pixel resolution of 2.5 *m* through image processing. We found that the northern end of WSD has been reduced by 2.1km over the past 15 years, and the southern end has been significantly shortened and rotated counterclockwise. Since 2011, the southern tip has been submerged in the water, and gradually disappeared at the average tide level. Over the past 15 years, the WSD sandbar has been shortened by about 5.7 km in length and rotated about 5 degrees counterclockwise. The southern shoreline of the sea side has gradually turned from a straight shape to an arc shape, and has a larger rotation than the northern section.

In terms of shoreline identification, the research team used image rotation to increase the amount of data by 18 times, and established three model structures. After the identification ability test, it was found that VGG16UNET is superior to the other two models The accuracy of the identification of the sea and land of WSD was as high as 90%. At the same time, VGG16UNET can effectively distinguish the sea and land areas covered by thin clouds and the land areas that are not in the training group. Because this VGG16UNET only uses 25 ground-truth images, the number of samples is not large enough. More images will be used in the future to have a refined AI model with more space-time applicability.

ACKNOWLEDGEMENTS

This article is part of the research project supported by the National Academy of Marine Research, No. NAMR109002. The author thanks the National Academy of Marine Research for funding support.

REFERENCES

Bayram, B., Janpaule, I., Oğurlu, M., Bozkurt, S., Reis, H. Ç., & Seker, D. Z. (2015). Shoreline Extraction and Change Detection Using 1:5000 Scale Orthophoto Maps: A Case Study of Latvia-Riga. *International Journal Environment Geoinformatics, 2*(3), 1-6. https://doi.org/10.30897/ijegeo.303552

Boak, E. H., & Turner, I. L. (2005). Shoreline definition and detection: a review. *Journal of coastal research, 21*(4), 688-703. https://doi.org/10.2112/03-0071.1

Chang, H. K., & Chen, W. W. (2005). Beach monitoring in Waisandin using satellite imagery. *Proceedings of the 27th Ocean Engineering Conference in Taiwan*, 823-830.

Chang, H. K., Lai, Y. C., & Chen, W. W. (2017). Shoreline Evolution of the Waisanding Barrier Using Waterline Detection from Satellite Images. *Journal of Photogrammetry and Remote Sensing, 22*(4), 243-262. https://doi.org/10.6574/JPRS.2017.22(4).2

Chen, W. W., & Chang, H. K. (2009). Estimation of Shoreline Position and Change from Satellite Images Considering Tidal Variation. *Estuarine, Coastal and Shelf Science, 84*(1), 54-60. https://doi.org/10.1016/j.ecss.2009.06.002

Cheng, D. C., Meng, G. F., Cheng, G. L., & Pan, C. H. (2016). SeNet: Structured Edge Network for Sea–Land Segmentation. *IEEE Geoscience and Remote Sensing Letters, 14*(2), 247-251. https://doi.org/10.1109/LGRS.2016.2637439

Dewi, R. S., Bijker, W., Stein, A., & Marfai, M. A. (2016). Fuzzy Classification for Shoreline Change Monitoring in a Part of the Northern Coastal Area of Java, Indonesia. *Remote Sensing, 8*(3), 190. https://doi.org/10.3390/rs8030190

Dickens, K., & Armstrong, A. (2019). Application of Machine Learning in Satellite Derived Bathymetry and Coastline Detection. *SMU Data Science Review, 2*(1), 4. https://scholar.smu.edu/datasciencereview/vol2/iss1/4

Foody, G. M. (2006). Pattern recognition and classification of remotely sensed images by artificial neural networks. In Recknagel, F. (eds), *Ecological Informatics* (pp. 459-477). Springer, Berlin, Heidelberg. https://doi.org/10.1007/3-540-28426-5_23

Fuse, T., & Ohkura, T. (2018). Development of Shoreline Extraction Method Based on Spatial Pattern Analysis of Satellite SAR Images. *Remote Sensing*, *10*(9), 1361. https://doi.org/10.3390/rs10091361

Gardel, A. & Gratiot, N. (2005). A Satellite Image-Based Method for Estimating Rates of Mud Banks Migration, French Guiana, South America. *Journal of Coastal Research, 21*(4), 720-728. https://doi.org/10.2112/03-0100.1

Ghoneim, E., Mashaly, J., Gamble, D., Halls, J., & AbuBakr, M. (2015). Nile Delta Exhibited A Spatial Reversal in the Rates of Shoreline Retreat on the Rosetta Promontory Comparing Pre- and Post-Beach Protection. *Geomorphology, 228*, 1-14. https://doi.org/10.1016/j.geomorph.2014.08.021

Gilvear, D., Tyler, A., & Davids, C. (2004). Detection of Estuarine and Tidal River Hydromorphology Using Hyper-Spectral and LiDAR Data: Forth Estuary, Scotland. *Estuarine, Coastal and Shelf Science, 61*(3), 379-392. https://doi.org/10.1016/j.ecss.2004.06.007

He, K., Zhang, X., Ren, S., & Sun, J. (2016). Deep Residual Learning for Image Recognition. *In Proceedings of the IEEE Conference on Computer Vision and Pattern Recognition*, 770-778. https://doi.org/10.48550/arXiv.1512.03385

Jishuang, Q., & Chao, W. (2002). A Multi-Threshold Based Morphological Approach for Extracting Coastal Line Feature in Remote Sensed Images. *International Archives of Photogrammetry, Remote Sensing and Spatial Information Sciences, 34*(1), 184-188. https://www.isprs.org/proceedings/XXXIV/part1/paper/00065.pdf

Kurosawa, T., & Tanaka, H. (2001). A Study of Detection of Shoreline Position with Aerial Photographs. *Proceedings of Coastal Engineering, JSCE, 48*, 586-590.

Li, R., Liu, W., Yang, L., Sun, S., Hu, W., Zhang, F., & Li, W. (2018). DeepUNet: A Deep Fully Convolutional Network for Pixel-Level Sea-Land Segmentation. *IEEE Journal of Selected Topics in Applied Earth Observations and Remote Sensing, 11*(11), 3954-3962. https://doi.org/10.48550/arXiv.1709.00201

Lin, T. Y., Lo, Y. F., & Hung, C. Y. (2007). Geomorphic Changes on the Barrier Islands of Southwestern Taiwan. *Proceedings of the 29th Ocean Engineering Conference in Taiwan*, 433-438.

Long, J., Shelhamer, E., & Darrell, T. (2015). Fully Convolutional Networks for Semantic Segmentation. *Proceedings of the IEEE Conference on Computer Vision and Pattern Recognition*, 3431-3440. https://doi.org/10.48550/arXiv.1411.4038

Milletari, F., Navab, N., & Ahmadi, S. A. (2016). V-net: Fully convolutional neural networks for volumetric medical image segmentation. *In 2016 fourth international conference on 3D vision (3DV)*, 565-571. https://doi.org/10.48550/arXiv.1606.04797

Peng, H. Y., Tseng, K. H., Chien, H., & Chen, Y. D. (2019). Utilizing Multitemporal Satellite Images to Investigate Topographical Changes of Waisanding Sandbar. *Taiwan Journal of Geoinfomatics, 7*(2), 103-119.

Ronneberger, O., Fischer, P., & Brox, T. (2015). U-Net: Convolutional Networks for Biomedical Image Segmentation. *In International Conference on Medical Image Computing and Computer-Assisted Intervention*, 234-241. https://doi.org/10.48550/arXiv.1505.04597

Ryu, J. H., Kim, C. H., Lee, Y. K., Won, J. S., Chun, S. S., & Lee, S. (2008). Detecting the Intertidal Morphologic Change Using Satellite Data. *Estuarin, Coastal and Shelf Science, 78*(4), 623-632. https://doi.org/10.1016/j.ecss.2008.01.020

Ryu, J. H., Won, J. S., & Min, K. D. (2002). Waterline Extraction from Landsat TM Data in a Tidal Flat: A Case Study in Gomso Bay, Korea. *Remote Sensing of Environment, 83*(3), 442-456. https://doi.org/10.1016/S0034-4257(02)00059-7

Shvets, A. A., Iglovikov, V. I., Rakhlin, A., & Kalinin, A. A. (2018). Angiodysplasia Detection and Localization Using Deep Convolutional Neural Networks. *In 2018 17th IEEE International Conference on Machine Learning and Applications*, 612-617. https://doi.org/10.1109/ICMLA.2018.00098

Simonyan, K., & Zisserman, A. (2014). Very Deep Convolutional Networks for Large-Scale Image Recognition, 1409-1556. https://doi.org/10.48550/arXiv.1409.1556

Su, J. C., Liu, C. I., Wang, K. F., Yu, C. W., Pan S.J., & Kuo, C.H. (2006). Investigation on the Morphologic Evolution of Yunlin Alongshore and Offshore Sand Bar. *Proceedings of the 28th Ocean Engineering Conference in Taiwan*, 587-591.

Toure, S., Diop, O., Kpalma, K., & Maiga, A. S. (2018). Coastline Detection Using Fusion of Over Segmentation and Distance Regularization Level Set Evolution. The International Archives of the Photogrammetry. *Remote Sensing and Spatial Information Sciences*, XLII-3/W4, 513-518. https://doi.org/10.5194/isprs-archives-XLII-3-W4-513-2018

Tsai, Y. N., Shi, G. Z., Chien, C. H., Kuo, C. A., & Yang, M. D. (2015). Study on the Topography Changing with Shoreline, Area and Volume at Wai-San-Ding Shoal. *Proceedings of the 37th Ocean Engineering Conference in Taiwan*, 361-366.

Wu, C. N., Hsiao, K. S., & Peng, M. H. (1991). Change Analysis of Waisandingzou. *Remote Sensing, 15*, 1-26.

Zhang, H. N., Jiang, Q. G., & Xu, J. (2013). Coastline Extraction Using Support Vector Machine from Remote Sensing Image. *Journal of Multimedia, 8*(2), 175-182. https://doi.org/10.4304/jmm.8.2.175-182